Molecular Pharmacology Fast Forward. Published on March 22, 2023 as DOI: 10.1124/molpharm.122.000601
This article has not been copyedited and formatted. The final version may differ from this version.

Determinants of subtype-selectivity of the anthelmintic paraherquamide A on *Caenorhabditis elegans* nicotinic acetylcholine receptors

Wataru Koizumi[1,#], Shuya Otsubo[1,#], Shogo Furutani[1,#], Kunihiro Niki[1,#], Koichi Takayama[1], Shota Fujimura[1], Takanobu Maekawa[1], Ryosuke Koyari[1], Makoto Ihara[1], Kenji Kai[2], Hideo Hayashi[2], Mohammad Shaokat Ali[3,4], Eriko Kage-Nakadai[3], David B. Sattelle[5] and Kazuhiko Matsuda[1,6,†]

[1]Department of Applied Biological Chemistry, Faculty of Agriculture, Kindai University, Nakamachi 3327-204, Nara, 631-8505, Japan

[2]Graduate School of Life and Environmental Sciences, Osaka Metropolitan University, 1-1 Gakuen-cho, Naka-ku, Sakai, Osaka 599-8531, Japan

[3]Graduate School of Human Life Science, Osaka Metropolitan University, 3-3-138 Sugimoto, Sumiyosi-ku, Osaka 558-8585, Japan

[4]Faculty of Food Science and Technology, Chattogram Veterinary and Animal Sciences University, Chattogram - 4225, Bangladesh

[5]Centre for Respiratory Biology, UCL Respiratory, Division of Medicine, University College London, London, WC1E 6JF, United Kingdom

[6]Agricultural Technology and Innovation Research Institute, Kindai University, Nakamachi 3327-204, Nara, 631-8505, Japan

[†]Corresponding author Kazuhiko Matsuda
Department of Applied Biological Chemistry, Faculty of Agriculture, Kindai University
3327-204 Nakamachi, Nara 631-8505, Japan
TEL: +81-742-437153: FAX: +81-742-43-1445
Email: kmatsuda@nara.kindai.ac.jp

[#]These authors contributed equally to this study.

Molecular Pharmacology Fast Forward. Published on March 22, 2023 as DOI: 10.1124/molpharm.122.000601
This article has not been copyedited and formatted. The final version may differ from this version.

Running title: Mechanism of selective action of paraherquamide A

Number of Text page:	45 Pages
Number of Tables	2 Tables
Number of Figures	7 Figures + 8 Supplemental Figures
Number of references	31 References
Number of words in Abstract	158 Words
Number of words in Introduction	723 Words
Number of words in Discussion	1045 Words

Abbreviations

ACh, acetylcholine; AChBP, acetylcholine binding protein; CI, confidence interval; EC_{50}, half maximal effective concentration; IC_{50}, half inhibition concentration; nAChR, nicotinic acetylcholine receptor; n_H, Hill coefficient; RMSD, root mean square deviation; SOS, standard oocyte saline.

Molecular Pharmacology Fast Forward. Published on March 22, 2023 as DOI: 10.1124/molpharm.122.000601
This article has not been copyedited and formatted. The final version may differ from this version.

Abstract

The anthelmintic paraherquamide A acts selectively on the nematode L-type nicotinic acetylcholine receptors (nAChRs) but the mechanism of its selectivity is unknown. This study targeted the basis of paraherquamide A selectivity by determining an X-ray crystal structure of the acetylcholine binding protein (AChBP), a surrogate nAChR ligand-binding domain, complexed with the compound and by measuring its actions on wild-type and mutant *Caenorhabditis elegans* nematodes and functionally expressed *C. elegans* nAChRs. Paraherquamide A showed a higher efficacy for the levamisole-sensitive (L-type (UNC-38/UNC-29/UNC-63/LEV8/LEV-1)) nAChR than the nicotine-sensitive (N-type (ACR-16)) nAChR, a result consistent with *in vivo* studies on wild type worms and worms with mutations in subunits of these two classes of receptors. The X-ray crystal structure of the *Ls*-AChBP-paraherquamide A complex and site-directed amino acid mutation studies showed for the first time that loop C, loop E and loop F of the orthosteric receptor binding site play critical roles in the observed L-type nAChR selective actions of paraherquamide A.

Molecular Pharmacology Fast Forward. Published on March 22, 2023 as DOI: 10.1124/molpharm.122.000601
This article has not been copyedited and formatted. The final version may differ from this version.

Significant statement

Paraherquamide A, an oxindole alkaloid, has been shown to act selectively on the L-type over N-type nAChRs in nematodes, but the mechanism of selectivity is unknown. We have co-crystallized paraherquamide A with the acetylcholine binding protein, a surrogate of nAChRs, and found that structural features of loop C, loop E and loop F contribute to the L-type nAChR selectivity of the alkaloid. The results create a new platform for the design of anthelmintic drugs targeting cholinergic neurotransmission in parasitic nematodes.

Molecular Pharmacology Fast Forward. Published on March 22, 2023 as DOI: 10.1124/molpharm.122.000601
This article has not been copyedited and formatted. The final version may differ from this version.

Introduction

Paraherquamide A (Figure 1A) is a polycyclic oxindole alkaloid, first isolated as a toxic metabolite from *Penicillium paraherquei* (Yamazaki et al., 1981). Its anthelmintic activity was demonstrated using gerbils (*Meriones unguiculatus*) infected with a parasitic nematode *Trichostrongylus colubriformi* (Ostlind et al., 1990) and in studies on the nematode genetic model organism *Caenorhabditis elegans* (Ondeyka et al., 1990). Subsequently, paraherquamide and related compounds were tested on a variety of parasitic nematodes, thereby establishing their broad spectrum anthelmintic activity (Lee et al., 2002).

Paraherquamide A and 2-deoxy-paraherquamide A (derquantel) induced rapid flaccid paralysis in the parasitic nematode *Haemonchus contortus* without affecting ATP concentration, indicating a possible action on nervous system or neuromuscular receptors (Thompson et al., 1996; Zinser et al., 2002). In the case of *H. contortus*, derquantel showed a higher paralytic activity than compound **1** and thus the mechanism of action of the deoxy-derivative was further examined using an *in vitro* assay. It reduced ACh-induced contraction of an *H. contortus* muscle strip in a manner similar to that seen with mecamylamine and methyllycaconitine, pointing to an action on cholinergic neuromuscular transmission (Zinser et al., 2002). Robertson et al (2002)

Molecular Pharmacology Fast Forward. Published on March 22, 2023 as DOI: 10.1124/molpharm.122.000601
This article has not been copyedited and formatted. The final version may differ from this version.

tested both paraherquamide A and derquantel for their capacity to block agonist-induced contraction of *Ascaris suum* muscle. Both compounds induced parallel shifts to the right of the ACh concentration-response curve, i.e. increased the EC_{50} values, indicating a competitive type of antagonism at nematode nAChRs (Robertson et al., 2002). The nicotine-sensitive (N-type), levamisole-sensitive (L-type) and bephenium-sensitive (B-type) nAChRs expressed on *Ascaris suum* body wall muscles were characterised and the blocking action of paraherquamide A and derquantel were investigated (Robertson et al., 1999). These studies confirmed that paraherquamide A blocked L-type receptors more effectively than N-type receptors in *A. suum*, whereas derquantel was most effective in blocking the B-type receptors, albeit with lower potency than paraherquamide A.

C. elegans is a genetic model organism with a fully sequenced genome and a comprehensive genetic toolkit (*C. elegans* Sequencing Consortium, 1998). The complete *C. elegans* nAChR subunit gene family has been identified (Jones et al., 2007) and the N-type (Ballivet et al., 1996; Boulin et al., 2008; Raymond et al., 2000) and L-type nAChRs (Boulin et al., 2008) have been expressed successfully in *Xenopus laevis* oocytes. A *C. elegans* receptor pharmacologically similar to the native L-type nAChR of *Ascaris suum* results from the co-expression of 8 genes (5x nAChR subunits

Molecular Pharmacology Fast Forward. Published on March 22, 2023 as DOI: 10.1124/molpharm.122.000601
This article has not been copyedited and formatted. The final version may differ from this version.

UNC-38, UNC-29, UNC-63, LEV-1 and LEV-8 co-expressed with 3x auxiliary proteins - RIC-3, UNC-50 and UNC-74), while a *C. elegans* equivalent of the *A. suum* N-type nAChR is obtained by co-expressing the nAChR ACR-16 with the expression-enhancing cofactor RIC-3 (Bennett et al., 2012; Boulin et al., 2008). Using recombinant nAChRs expressed functionally with the aid of auxiliary proteins, the actions of agonists levamisole, pyrantel and tribendimidine as well as the antagonist derquantel have been described for nAChRs from the important porcine nematode parasite *Oesophagostomum dentatum* (Buxton et al., 2014). Changes in both EC_{50} and maximum nAChR response were observed by adding UNC-38 and LEV-8 to the UNC-63/UNC-29 nAChR. The *C. elegans* L-type 2.1 (UNC-38/UNC-29/UNC-63/LEV-1/ACR-8) and 2.2 (UNC-38/UNC-29/UNC-63/ACR-8) nAChRs were employed to show that the ACR-8 subunit has the capacity to substitute for LEV-8 in the L-type nAChR when expressed in *X. laevis* oocytes (Blanchard et al., 2018). Binding of [^{3}H]paraherquamide A to *C. elegans* membranes was displaced by phenothiazines, members of a previous generation of anthelmintics, suggesting the possibility of a similar site of action (Schaeffer et al., 1992). Omitting ACR-8 from UNC-38/UNC-29/UNC-63/ACR-8 nAChRs was shown to change the action of derquantel from competitive to non-competitive (Buxton et al., 2014). However, the

Molecular Pharmacology Fast Forward. Published on March 22, 2023 as DOI: 10.1124/molpharm.122.000601
This article has not been copyedited and formatted. The final version may differ from this version.

molecular mechanism underpinning the higher efficacy of these ligands for the L-type than the N-type nAChR remains unknown.

Here we have investigated the mechanism of actions of paraherquamide A on the *C. elegans* N-type (ACR-16) and L-type (UNC-38/UNC-29/UNC-63/LEV-1/LEV-8) nAChRs expressed in *X. laevis* oocytes to address its subtype selectivity and to examine whether it shows competitive or non-competitive actions on *C. elegans* nAChRs. Also, we co-crystallized paraherquamide A with the acetylcholine binding protein from *Lymnaea stagnalis* (*Ls*-AChBP) to elucidate how the ligand-binding, orthosteric site interacts with the compound. We found that paraherquamide A is a much more potent antagonist of the L-type compared to the N-type *C. elegans* nAChR and explored structural features of the nematode nAChR subunits contributing to the L-type nAChR selectivity of the compound.

Molecular Pharmacology Fast Forward. Published on March 22, 2023 as DOI: 10.1124/molpharm.122.000601
This article has not been copyedited and formatted. The final version may differ from this version.

Materials and Methods

Chemicals

Paraherquamide A was purified *de novo* from the fermentation products of *Penicillium sp.* OK188 strain as follows. The *Penicillium* culture was inoculated with 8 kg of the okara medium and incubated at 25ºC for 1 week. The fermentation products were extracted with 1 L of methanol. The methanol extract was partitioned with an equal volume of ethyl acetate and the ethyl acetate layer was evaporated to yield 34.2 g of residue, which was dissolved in a minimal amount of methanol and partitioned with hexane. The remaining methanol layer was partitioned with ethyl acetate and the ethyl acetate layer was evaporated to dryness. The residue (5.06 g) was purified using silica gel column chromatography (C-200, Wako Pure Chemical Industries, Osaka, Japan) with ethyl acetate-methanol mixture (Stepwise increase of methanol concentration (5, 10, 20 and 50%)). Paraherquamide A, which is detected as an orange spot by UV absorption on a TLC plate, was eluted by an ethyl acetate-methanol mixture with stepwise increase of methanol concentration (0, 5, 10, 20, 50%). Fractions eluted by ethyl acetate containing methanol 0, 5 and 10% were collected and evaporated to yield 2.49 g residue, which was purified by silica gel column chromatography using a hexane–acetone mixture with stepwise increase of the acetone concentration (0, 10, 20,

Molecular Pharmacology Fast Forward. Published on March 22, 2023 as DOI: 10.1124/molpharm.122.000601
This article has not been copyedited and formatted. The final version may differ from this version.

30, 40, 50, 60, 70, 80, 90, 100%). Fractions eluted with hexane containing 50 and 60% acetone were evaporated to obtain an 800 mg residue, which was further purified by silica gel column chromatography using a chloroform–methanol mixture with stepwise increase of methanol concentration (0, 0.1, 0.2, 0.3, 0.4, 0.5, 0.6, 0.7, 0.8, 0.9, 1, 2, 5, 10%). Fractions eluted with chloroform containing 0.2, 0.3, 0.4 and 0.5% methanol were collected, and the solvents were evaporated. The resultant solid was re-crystallized in ethanol (Yield, 157.6 mg) and this re-crystallised material was dissolved in methanol to further purify by a preparative HPLC (VP-10 series, Shimadzu, Japan) using a Unison US-C18 column (20 x l50 mm, Imtakt, Japan) with methanol–water mixture (4:1) at a flow rate of 7.5 mL min^{-1} (Yield, 25. 3 mg; Purity was confirmed to be >99% by HPLC, Figure S1).

Spectral data of Paraherquamide A

Specific rotation ($[\alpha]_D^{25}$) of paraherquamide A was determined using a SEPA-300 polarimeter (Horiba, Japan) to be = -17.3 (*c* = 0.2, methanol). Electrospray Ionization–mass of the compound was measured using a Q-Tof Premier (Waters, USA) with a 2-propanol/50 mM aqueous NaOH solution containing 0.5% formic acid = 9/1). The observed mass (M+1) was 494.2660 (calculated to be 494.2665 for $C_{28}H_{36}O_5N_3$). The ^{1}H- and ^{13}C-NMR spectra were measured in $CDCl_3$ using an Avance System,

Molecular Pharmacology Fast Forward. Published on March 22, 2023 as DOI: 10.1124/molpharm.122.000601
This article has not been copyedited and formatted. The final version may differ from this version.

UltraShield 400 Plus (Bruker BioSpin, USA) (Figures S2, S3). Chemical shifts δ (ppm) (splitting patterns and coupling constants (Hz)) of the ^{1}H-NMR spectrum (Figure S2) were 0.83 (3H, s, H-23), 1.07 (3H, s, H-22), 1.41 (3H, s, H-28), 1.42 (3H, s, H-27), 1.62 (3H, s, H-17), 1.73~1.91 (4H, m, H-10b, H-15a, H-19a, H-19b) , 2.23 (1H, ddd, J= 4.7, 9.1, 10.8 Hz, H-16b), 2.35 (1H, ddd, J= 4.5, 10.8, 13.3 Hz, H-15b), 2.55 (1H, dd, J= 1.4, 11.2 Hz, H-12b), 2.63 (1H, br s, 14-OH), 2.68 (1H, d, J= 15.3 Hz, H-10a), 3.00 (1H, dd, J=1.5, 11.1 Hz, H-20), 3.03 (3H, s, H-29), 3.21 (1H, ddd, J= 4.5, 9.0, 9.1 Hz, H-16a), 3.60 (1H, d, J=11.2, H-12a), 4.87 (1H, d, J=7.7 Hz, H-25), 6.30 (1H, d, J=7.6 Hz, H-24), 6.67 (1H, d, J=8.0 Hz, H-5), 6.79 (1H, d, J=8.1 Hz, H-4), 7.62 (1H, s, H-N1). Chemical shifts δ (ppm) of the ^{13}C-NMR spectrum (Figure S3) were 19.1 (C-17), 20.4 (C-22), 22.0 (C-19), 23.6 (C-23), 25.9 (C-29), 29.7 (C-28), 29.9 (C-27), 37.0 (C-10), 38.0 (C-15), 46.3 (C-21), 51.4 (C-20), 51.8 (C-16), 59.0 (C-12), 63.0 (C-3), 65.2 (C-11), 71.3 (C-13), 78.0 (C-14), 79.7 (C-26), 115.0 (C-25), 117.2 (C-5), 120.3 (C-4), 124.9 (C-9), 132.4 (C-8), 135.2 (C-7), 138.9 (C-24), 146.0 (C-6), 171.3 (C-18), 182.6 (C-2). These NMR spectral data were in agreement with those reported previously (Blanchflower et al., 1991).

ACh chloride, levamisole and (-)-nicotine were purchased from MilliporeSigma (USA). Derquantel was purchased from Santa Cruz Biotechnology (USA). These compounds were >95% pure.

Molecular Pharmacology Fast Forward. Published on March 22, 2023 as DOI: 10.1124/molpharm.122.000601
This article has not been copyedited and formatted. The final version may differ from this version.

cRNA preparation

The cRNAs encoding the *C. elegans* nAChR subunits and auxiliary proteins RIC-3, UNC-50 and UNC-74 were prepared using the mMESSAGE mMACHINE T7 ULTRA kit (Thermo Fisher Scientific, USA) from their cDNAs (Accession number: ACR-16, AY523511.1; UNC-38, X98600.1; UNC-29, NM_059998.4; UNC-63, AF288374.1; LEV-1, X98601.1; LEV-8, NM_077531.4; ACR-8, NM_001375112; RIC-3, NM_068898.4; UNC-50, NM_066878.3; UNC-74, accession number not determined). The cDNAs encoding the L-type nAChR subunits UNC-38, UNC-29, UNC-63, LEV-1, LEV-8, as well as those encoding the auxiliary proteins RIC-3, UNC-50 and UNC-74 were gifts from Prof. Thomas Boulin. The cRNAs were dissolved in RNase-free water and mixed at a final concentration of 50 ng μL^{-1} of each subunit and auxiliary protein. Then 50 nL of this RNA mixture solution was injected into *X. laevis* oocytes. When measuring the effects of (-)-nicotine and levamisole on the YPSCC mutant of the N-type nAChR, the RNA concentration was 500 ng μL^{-1} to confirm that they had no agonist action on this nAChR (See below for the results).

Expression of *C. elegans* nAChRs in *Xenopus laevis* oocytes

An ethic statement for experiments using the frogs is not required in Japan but as a UK scientist was involved, all our experiments followed the standards of the UK

Molecular Pharmacology Fast Forward. Published on March 22, 2023 as DOI: 10.1124/molpharm.122.000601
This article has not been copyedited and formatted. The final version may differ from this version.

legislation. Oocytes (stage V or VI) were excised from female *X. laevis* anesthetized by benzocaine according to the U. K. Animals (Scientific Procedures) Act, 1986. We also minimized the use of frogs as much as possible. After treating the excised oocytes for 15 min with 2.0 mg mL^{-1} collagenase (Type IA, MilliporeSigma) in Ca^{2+}-free standard oocyte saline (SOS) containing100 mM NaCl, 2 mM KCl, 1 mM $MgCl_2$ and 5 mM HEPES 5.0 (pH 7.6), they were moved into SOS consisting of 100 mM NaCl, 2 mM KCl, 1.8 mM $CaCl_2$, 1 mM $MgCl_2$ and 5 mM HEPES 5.0 (pH 7.6). The follicle cell layer was removed and the cytoplasm of defolliculated oocytes was injected with 50 nL of the cRNA solution mix encoding either the N-type nAChR (ACR-16 with accessory protein RIC-3), or the L-type nAChR (UNC-38, UNC-29, UNC-63, LEV-1, LEV-8 with the accessory proteins RIC-3, UNC-74 and UNC-50) and incubated at 18°C in SOS supplemented with penicillin (100 units mL^{-1}), streptomycin (100 µg mL^{-1}), gentamycin (50 µg mL^{-1}), 2.5 mM sodium pyruvate and 4% horse serum for 2–5 days prior to electrophysiological experiments.

Voltage-clamp electrophysiology

The ACh-induced nAChR responses were recorded in SOS containing 0.5 µM Atropine (SOS-A), which was added to suppress any possible endogenous muscarinic responses, at 18–23°C (Matsuda et al., 1998). Oocytes were secured in a recording

Molecular Pharmacology Fast Forward. Published on March 22, 2023 as DOI: 10.1124/molpharm.122.000601
This article has not been copyedited and formatted. The final version may differ from this version.

chamber and perfused with SOS-A at a flow rate of 7–10 mL min^{-1}. Membrane currents were recorded at a holding potential of -100 mV. The electrodes were filled with 2 M KCl and had a resistance of 0.3 – 5 MΩ in SOS-A. Signals were digitised at a frequency of 1 kHz, recorded and analyzed using with pCLAMP software (Molecular Devices, USA). ACh was dissolved in SOS-A, while paraherquamide A was dissolved in dimethyl sulfoxide at 10 mM and then diluted with SOS-A immediately prior to experiments. DMSO concentrations in test solutions were 0.1% or lower, at which the solvent had no effect on the nAChR response to ACh and the actions of paraherquamide A. ACh was applied to oocytes for 3 – 5 s, with an interval of 3 min between applications. When testing the blocking action of paraherquamide, ACh was first applied several times until the oocyte response amplitude became stable. Then paraherquamide A was applied for 1 min prior to co-applications with ACh.

Analysis of current data

The amplitude of the ACh-induced current was normalized to that of the response at which it reached a plateau (I_{max}). The ACh concentration–response curves in the presence and absence of paraherquamide A and the paraherquamide A concentration-inhibition curves were fitted with equation (1) and (2), respectively, using Prism 6 (GraphPad Software, USA):

Molecular Pharmacology Fast Forward. Published on March 22, 2023 as DOI: 10.1124/molpharm.122.000601
This article has not been copyedited and formatted. The final version may differ from this version.

$$Y = \frac{I_{max}}{1+10^{(\log EC_{50}-[L])n_H}} \qquad (1)$$

$$Y = \frac{1}{1+10^{([L]-\log IC_{50})}} \qquad (2)$$

where Y is the normalized response, I_{max} is the normalized maximum ACh response, EC_{50} (M) is the half maximal effective concentration, IC_{50} (M) is the half inhibition concentration (M), [L] is the logarithm of the concentration of ligand (M) and n_H is the Hill coefficient.

Toxicity of paraherquamide A on *C. elegans*

C. elegans [Strains N2 (Wild type), RB918 *acr-16* (*ok789*) V (N-type nAChR mutant), ZZ20 *unc-38* (*x20*) I (L-type nAChR mutant), ZZ37 *unc-63* (*x37*) I (L-type nAChR mutant)] were obtained from the Caenorhabditis Genetics Center. Effects of the compounds on swimming (thrashing movements) of the worms were investigated as previously reported (Ondeyka et al., 1990). pLC_{50} values (=-logLC_{50}), where LC_{50} is the half lethal concentration (M)) for paraherquamide A on the wild type and mutant worms, were determined by non-linear regression with Prism 6 according to equation (2) in which IC_{50} is replaced by LC_{50}.

Molecular Pharmacology Fast Forward. Published on March 22, 2023 as DOI: 10.1124/molpharm.122.000601
This article has not been copyedited and formatted. The final version may differ from this version.

Crystallization of *Ls*-AChBP complexed with paraherquamide A

The wild type *Ls*-AChBP was expressed in the yeast *Pichia pastoris* X-33 strain as described previously (Ihara et al., 2014). Secreted proteins were concentrated using a Vivaflow 200 Cross Flow Cassette (Sartorius, Germany) and purified with a Source 30Q column (Cytiva, USA). The *Ls*-AChBP was treated overnight at 37°C with His-tagged endo-β-*N*-acetylglycosidase H (Endo H, gene accession number K02182), where Endo H was expressed in *Escherichia coli* BL21 (DE3) and purified by Ni-NTA column chromatography. The protein was further purified with a Mono Q column followed by a Superdex 200 (Cytiva). Purified *Ls*-AChBP was dialyzed over 20 mM Tris-HCl buffer (pH 7.5) and its concentration adjusted to 5.0 mg/mL. The *Ls*-AChBP complexed with paraherquamide A was crystallized by sitting drop vapor diffusion method. Crystals of the complex were flash cooled in liquid nitrogen and stored in liquid nitrogen prior to X-ray diffraction data collection.

X-ray crystallography

X-ray diffraction data were collected at 100 K with a RAYONIX MX225HE detector at BL26B1 located at SPring-8, the third-generation synchrotron facility in Harima Science Park City, Hyogo, Japan. Diffraction data were processed using the Aimless (CCP4: supported program)(Evans and Murshudov, 2013; Winn et al., 2011)

Molecular Pharmacology Fast Forward. Published on March 22, 2023 as DOI: 10.1124/molpharm.122.000601
This article has not been copyedited and formatted. The final version may differ from this version.

along with XDS(Kabsch, 2010). The initial phase was obtained by molecular replacement with PHASER(McCoy, 2007) using a protein coordinate: 2ZJU. Refinement of the structure model was performed using Refmac5 (Murshudov et al., 2011), and manual model building was performed with Coot (Emsley and Cowtan, 2004). Two-dimensional figures and cartoon/stick models of the crystal structure of the *Ls*-AChBP-paraherquamide A complex were illustrated by LIGPLOT (Wallace et al., 1996) and PyMoL (Schrödinger, USA), respectively.

Modeling proteins in complex with ligands

Prior to modelling, structure coordinates of paraherquamide A and derquantel were prepared using Chem3D software and AutoDock Tools 1.5.7. Derquantel was docked into *Ls*-AChBP after removing water and paraherquamide A from the X-ray crystal structure of the protein complexed with paraherquamide A. For modeling the ACR-16 protein complexed with paraherquamide A, ACR-16 was aligned with *Ls*-AChBP using MAFFT 7.308 (Katoh et al., 2002; Katoh and Standley, 2013). Then, the aligned region corresponding to amino acid number 23 − 228 of *C. elegans* ACR-16 was modeled with MODELLER 10.1 using the AutoModel algorithm(Webb and Sali, 2016). Paraherquamide A was docked into the homology model of wild type ACR-16 using AutoDock Vina 1.1.2(Trott and Olson, 2010).

Molecular Pharmacology Fast Forward. Published on March 22, 2023 as DOI: 10.1124/molpharm.122.000601
This article has not been copyedited and formatted. The final version may differ from this version.

Statistical analysis

Differences of the means were analyzed by parametric methods (*t*-test (two-tailed), or one-way ANOVA (Dunnett test)) in which post hoc tests were conducted only when *F* values were < 0.05. The difference compared was judged significant at $p < 0.05$ level.

Results

Actions of paraherquamide A on N-type and L-type *C. elegans* nAChRs

First, we tested paraherquamide A alone on oocytes expressing either the N-type (ACR-16) or the L-type (UNC-38/UNC-29/UNC-63/LEV-1/LEV-8) *C. elegans* nAChRs. Paraherquamide A had no detectable effect on the membrane currents when applied at 10 μM (Figure 1B, C), indicating that it had no detectable agonist action on either receptor at this concentration. Next, we perfused nAChR-expressing oocytes with paraherquamide A (N-type, 10 μM; L-type, 100 nM) for 1 min prior to applying ACh at 100 μM. These paraherquamide A exposures reduced the ACh response of N-type and L-type nAChRs by 31.6 (95% confidence interval (95% CI): 14.5 – 48.8) and 76.4 (95% CI: 68.0 – 84.8), respectively (Figure 1B, C). We evaluated the antagonist potency of

Molecular Pharmacology Fast Forward. Published on March 22, 2023 as DOI: 10.1124/molpharm.122.000601
This article has not been copyedited and formatted. The final version may differ from this version.

paraherquamide A by treating oocytes expressing the N-type nAChR with the alkaloid for 1 min and then co-applying ACh at 10 μM, which is close to the EC_{50} for ACh (Table 1). Paraherquamide A reduced the peak ACh response of the N-type nAChR with a pIC_{50} (= -logIC_{50} (M)) of 4.84 (95% CI: 4.76 − 4.91) (Figure 1D, Table 1).

In a similar way, we also treated oocytes expressing the L-type (UNC-38/UNC-29/UNC-63/LEV-1/LEV-8) nAChR with paraherquamide A for 1 min prior to co-application with 30 μM ACh. Paraherquamide A also reduced the peak current amplitude of the ACh response of the L-type nAChR with a pIC_{50} of 7.58 (95% CI: 7.51 − 7.64) (Figure 1E, Table 1). The nAChR blocking potency measured as pIC_{50} was higher for the L-type nAChR compared to the N-type nAChR. Derquantel also blocked the ACh-responses of the N-type (ACR-16) and L-type (UNC-38/UNC-29/UNC-63/LEV-1/LEV-8) nAChRs (N-type, pIC_{50} values of 4.76 (95% CI: 4.63 − 4.89); L-type 6.03 (95% CI: 5.94 − 6.11) with preference to L-type over N-type nAChRs (Figure S4). Since paraherquamide A was 35.5-fold more potent on the L-type nAChR than derquantel, we focused on the mechanism of selectivity of paraherquamide A to the *C. elegans* L-type over N-type nAChRs.

Prior to investigating the effects of paraherquamide A, we first measured the concentration-response curves for ACh for the N-type (ACR-16) and L- type

Molecular Pharmacology Fast Forward. Published on March 22, 2023 as DOI: 10.1124/molpharm.122.000601
This article has not been copyedited and formatted. The final version may differ from this version.

(UNC-38/UNC-29/UNC-63/LEV-1/LEV-8) nAChRs. ACh activated the N-type nAChR with pEC_{50} (= $-logEC_{50}$) of 4.67 (95% CI: 4.63 − 4.70) (Figure 1F, Table 1), whereas it activated the L-type nAChR with pEC_{50} of 4.39 (95% CI: 4.34 − 4.44) (Figure 1G, Table 1). These data are comparable to those reported previously (Boulin et al., 2008). We then investigated the effects of 10 μM paraherquamide A on the ACh concentration-response curve for the N-type nAChR. The compound shifted the ACh concentration-response curve to the right (pEC_{50} = 4.35 (95% CI: 4.18 − 4.52), $P < 0.05$, two-tailed *t*-test) and reduced the amplitude of the normalized maximum response (I_{max} = 0.453 (95% CI: 0.395 − 0.510), $P < 0.05$, two-tailed *t*-test) (Figure 1F), suggesting mixed competitive and non-competitive interactions with the N-type nAChR. On the other hand, 100 nM paraherquamide A reduced the maximum response of the L-type nAChR (I_{max} = 0.300 (95% CI: 0.190 − 0.409), $P < 0.05$, two-tailed *t*-test), while hardly shifting pEC_{50} (4.27 (95% CI: 3.75 − 4.79)) (Figure 1G), indicating non-competitive interactions with the L-type nAChR.

To examine the role of the L-type nAChR subunits UNC-38, UNC-29, UNC-63, LEV-1 and LEV-8 in determining paraherquamide A sensitivity, we tested the compound on the L-type 2.1 (UNC-38/UNC-29/UNC-63/LEV-1/ACR-8) and 2.2 (UNC-38/UNC-29/UNC-63/ACR-8) nAChRs. Replacing the LEV-8 subunit by the ACR-8

Molecular Pharmacology Fast Forward. Published on March 22, 2023 as DOI: 10.1124/molpharm.122.000601
This article has not been copyedited and formatted. The final version may differ from this version.

subunit had a minimal impact on the concentration-response curve for ACh (Figure 1H). However, omitting the LEV-1 subunit shifted it (Figure 1I). The 2.1 nAChR showed lower paraherquamide A sensitivity than the L-type (UNC-38/UNC-29/UNC-63/LEV-1/LEV-8) nAChR but >100-fold higher sensitivity than the N-type (ACR-16) nAChR (Figure 1J, Table 1). Omitting the LEV-1 subunit from the 2.2 nAChR had a minimal impact on the paraherquamide sensitivity (Figure 1K, Table 1).

Actions of paraherquamide A on wild type and mutant *C. elegans*

We investigated the effects of paraherquamide A on thrashing of wild-type and mutant *C. elegans* to confirm its selectivity for the L-type nACR *in vivo*. The compound suppressed thrashing of the wild type worms with pLD_{50} of 5.02 (95% CI: 4.91 − 5.12) (Figure 2A). Paraherquamide A inhibited thrashing of *C. elegans* with a mutation in the ACR-16 subunit (RB918 *acr-16* (*ok789*) V) with pLC_{50} of 5.61 (95% CI: 5.52 − 5.69) (Figure 2B), showing higher paraherquamide A sensitivity than the wild type worms. We failed to determine the activity on the UNC-38 mutant (ZZ20 *unc-38* (*x20*) I) because of its considerably reduced motility even in the absence of the compound, although we could measure activity on worms with a mutation in the *unc-63* gene (ZZ37 *unc-63* (*x37*) I). The UNC-63 mutant worms were highly resistant to paraherquamide A (Figure 2C), confirming a preference of the compound for L-type over N-type AChRs.

Molecular Pharmacology Fast Forward. Published on March 22, 2023 as DOI: 10.1124/molpharm.122.000601
This article has not been copyedited and formatted. The final version may differ from this version.

X-ray crystal structures of *Ls*-AChBP in complex paraherquamide A

The AChBPs have been used to investigate the mechanism of action of various ligands interacting with the orthosteric sites of nAChRs. Having observed the competitive paraherquamide A interactions with ACh at the N-type nAChR (Figure 1F), we co-crystallized paraherquamide A with the *Ls*-AChBP. When crystallized in 14.1-15.6% PEG 4000 in sodium citrate buffer (pH 5.0) at 20°C, the *Ls*-AChBP-paraherquamide A complex resulted in a crystal with a space group of P65 at a resolution of 2.2 Å (Table 2). We therefore modelled its crystal structure with the amino acid sequence shown in Figure 3A. The electron densities for the ligand were observed at all five interfaces between protomers (Figure 3B; see Figure S5 for detailed omit maps). Paraherquamide A interacted with the *Ls*-AChBP at ligand binding loops A, B, C, D, E and F (Figure 3C). The Ser186 and mainchain of Cys187 in loop C as well as hydroxy group of Tyr164 in loop F formed hydrogen bonds via a water with the carbonyl group in the amide bond of paraherquamide A (Figure 3C, D). The mainchain of Trp143 in loop B formed a hydrogen bond with the bridgehead nitrogen of paraherquamide A (Figure 3C, arrowed). Tyr192 in loop C and the main chain carbonyl of Trp143 in loop B formed hydrogen bonds with the hydroxy group of paraherquamide A (Figure S6). Trp53 (loop D), Tyr89 (loop A), Met114 (loop E), Tyr185 (loop C) and Tyr192 (loop C) made

Molecular Pharmacology Fast Forward. Published on March 22, 2023 as DOI: 10.1124/molpharm.122.000601
This article has not been copyedited and formatted. The final version may differ from this version.

hydrophobic contacts with the compound (Figure 3C, E). In loop C, UNC-38, UNC-63 and LEV-8 of the L-type nAChR have a proline, while ACR-16 N-type nAChR subunit has an aspartate (Figure 3A). In loop E, UNC-38 of the L-type nAChR has Glu142, which corresponds to Met114 in the *Ls*-AChBP (Figure 3A), has a negative charge favourable for interactions with a nitrogen of paraherquamide A (Figure 3C, E), whereas ACR-16 has Val138 with no negative charge at the corresponding position.

The effects of mutations in loop C and E of N- and L-type nAChRs on the actions of paraherquamide A, (-)-nicotine and levamisole

To examine whether loop C interacts with paraherquamide A as in the crystal structure of the *Ls*-AChBP complex, we investigated the effects of replacing its YDCC sequence in loop C of ACR-16 (N-type nAChR) by the YPSCC sequence of UNC-38 (L-type nAChR) on paraherquamide A actions (see Figure 3A for amino acid sequence comparisons). Switching this loop C segment lowered the pEC_{50} value of ACh to 4.01 (95% CI: 3.95 − 4.06) (Figure 4A, Table 1). The pIC_{50} of paraherquamide A determined in terms of reduction of the response to 100 μM ACh was increased significantly by the mutation to 5.28 (95% CI: 5.20 − 5.36) (Figure 4B, Table 1). A reciprocal loop C switch in the UNC-38 of the L-type nAChR, replacing the YPSCC sequence by the YDCC sequence of the N-type (AChR-16) nAChR subunit, had a minimal effect on the agonist

Molecular Pharmacology Fast Forward. Published on March 22, 2023 as DOI: 10.1124/molpharm.122.000601
This article has not been copyedited and formatted. The final version may differ from this version.

potency of ACh (Figure 4C, Table 1). However, the mutation reduced the antagonist potency of paraherquamide A to 7.37 (95% CI: 7.28 − 7.47) (Figure 4D, Table 1). Further, loop C of ACR-16 was mutated from YDCC to YPCC, as seen in UNC-63, resulting in enhanced paraherquamide A sensitivity to pIC_{50} of 5.54 (95% CI: 5.43 − 5.65) (Figure 4B, Table 1). In contrast, replacing the loop C of UNC-63 L-type nAChR subunit from YPCC by YDCC seen in AChR-16 subunit reduced sensitivity (pIC_{50} = 7.31 (95% CI: 7.23 − 7.38), Figure 4D, Table 1).

As described above, Met114 in loop E was in the vicinity of the bridgehead nitrogen of paraherquamide A in the crystal structure of the *Ls*-AChBP (Figure 3E). Since Met114 corresponds to Val138 and Glu142 in the ACR-16 (N-type nAChR) and UNC-38 (L-type nAChR) subunits, respectively (Figure 3A), Val138 was mutated to glutamate in the ACR-16 subunit. As a result, the antagonist potency in terms of pIC_{50} of paraherquamide A on the N-type nAChR was increased to 5.21 (95% CI: 5.11 − 5.31), while the agonist potency, monitored as pEC_{50} of ACh, was reduced to 3.24 (95% CI: 3.16 − 3.33) (Figure 4E, F, Table 1). By contrast, an inverse mutation E142V in UNC-38 subunit reduced the antagonist potency of paraherquamide A on the L-type nAChR (pIC_{50} =7.15 (95% CI: 7.03 − 7.27)), while scarcely influencing the agonist potency of ACh (Figure 4G, H, Table 1).

Molecular Pharmacology Fast Forward. Published on March 22, 2023 as DOI: 10.1124/molpharm.122.000601
This article has not been copyedited and formatted. The final version may differ from this version.

We also tested the effects of these mutations on the agonist actions of (-)-nicotine and levamisole and on the antagonist actions of paraherquamide A on responses to these ligands of the N-type and L-type nAChRs (Figure 5). (-)-Nicotine activated the wild type N-type nAChR with pEC_{50} of 4.73 (95% CI: 4.64 − 4.83) (Figure 5A, Figure S7A) and paraherquamide A inhibited the nicotine-induced response with pIC_{50} of 5.48 (95% CI: 5.35 − 5.61) (Figure S7B). However, all the mutations tested abolished the agonist action of (-)-nicotine on the N-type (ACR-16) nAChR (Figure 5A) and did not make it an agonist of the L-type (UNC-38/UNC-29/UNC-63/LEV-1/LEV-8) nAChR (Figure 5B).

Levamisole did not activate the wild type, nor the mutant N-type nAChRs (Figure 5C), while activating, not only the wild type, but also the mutant L-type nAChRs with no significant difference in pEC_{50} (Figure 5D, E, F, G, H). However, the YDCC mutation in loop C of UNC-63 and the E142V mutation in loop E of UNC-38 reduced I_{max} (Figure 5E, F, Table S1). The mutations tested hardly affected pIC_{50} of paraherquamide A on the response to levamisole (Figure 5G, H).

The effects of the mutations in loop C and loop E on IC_{50} values for paraherquamide A acting on the L-type (UNC-38/UNC-29/UNC-63/LEV-1/LEV-8) nAChR, albeit significant, were not as large as those observed for the corresponding

Molecular Pharmacology Fast Forward. Published on March 22, 2023 as DOI: 10.1124/molpharm.122.000601
This article has not been copyedited and formatted. The final version may differ from this version.

mutations in the N-type (ACR-16) nAChR (Figure 4, Table 1). Therefore, it is conceivable that other structural features may also underlie the L-type nAChR selectivity of the compound. Referring to the homology model of the N-type nAChRs in complex with paraherquamide A (Figure 6), we postulated that Asp210 in loop C and Phe184 in loop F, both of which are only seen in the ACR-16 subunit (Figure 3A), may contact each other, indirectly interrupting with loop C−paraherquamide A interactions. No such steric interaction occurs between the proline residue in the α subunits and valine residues in the non-α subunits (UNC-29, LEV-1) in the L-type nAChR (Figure 3A), strengthening interactions with the alkaloid. To test this hypothesis, we mutated Phe184 to valine in loop F of ACR-16 and measured the blocking potency of paraherquamide A on the mutant N-type nAChR (Figure 7). We found that the mutation hardly affected the potency of ACh, while increasing pIC_{50} of paraherquamide A for the N-type nAChR (Figure 7, Table 1). By contrast, both the V193F mutation in UNC-29 and the V201F mutation in LEV-1 reduced the blocking potency of paraherquamide A (Figure 7, Table 1). On the other hand, the F184V mutation in the N-type nAChR and the V193F mutation (UNC-29) and V201F mutation (LEV-1) in the L-type nAChR had a limited impact on the agonist activity of (-)-nicotine and levamisole, respectively (Figure S8).

Molecular Pharmacology Fast Forward. Published on March 22, 2023 as DOI: 10.1124/molpharm.122.000601
This article has not been copyedited and formatted. The final version may differ from this version.

Discussion

We have investigated the antagonist actions of pararherquamide A on recombinant *C. elegans* N-type (ACR-16) and L-type (UNC-38/UNC-29/UNC-63/LEV-1/LEV-8) nAChRs expressed in *Xenopus laevis* oocytes. The L-type nAChR showed a higher paraherquamide A sensitivity compared to the N-type nAChR with a difference in pIC_{50} of 2.74 (an approximately 550-fold change in IC_{50}, Figure 1D, E, Table 1), consistent with findings for the *Ascaris suum* N- and L- type nAChRs (Robertson et al., 2002). Also, the tests of the compound on the L-type 2.1 and 2.2 nAChRs (Figure 1J, K) and the wild type and mutant *C. elegans* worms (Figure 2) suggest that the higher paraherquamide sensitivity of the L-type nAChR compared to the N-type nAChR appears to hold for nAChRs of a parasitic (*A. suum*) and a free-living (*C. elegans*) nematode.

Paraherquamide A interacted competitively with ACh on the N-type nAChRs of *C. elegans* (Figure 1F), as is the case of native *Ascaris suum* nAChRs (Robertson et al., 2002), suggesting that the compound binds to the orthosteric site. Its non-competitive antagonist action on the *C. elegans* L-type nAChR does not exclude interactions with the orthosteric site, because such an action can result from binding to a distinct orthosteric site from that to which ACh is bound among the orthosteric α subunit/α

Molecular Pharmacology Fast Forward. Published on March 22, 2023 as DOI: 10.1124/molpharm.122.000601
This article has not been copyedited and formatted. The final version may differ from this version.

subunit and α subunit/non-α subunit interfaces in the L-type nAChR. Alternatively, paraherquamide A may lock the nAChR to an inactive state and prevent its activation by ACh, resulting in an apparent non-competitive interaction as in the case of the α7 nAChR interactions with α-bungarotoxin, where the toxin allosterically inhibits the ACh-induced activation of the nAChR even though both ligands share the orthosteric site (daCosta et al., 2015).

Given the similarity to the orthosteric site of the N-type (ACR-16) nAChR in forming a homo-pentameric structure and the competitive interaction of the ACR-16 homomer with paraherquamide A, *Ls*-AChBP was used as a nAChR ligand binding domain surrogate for co-crystallization studies with the fungal alkaloid paraherquamide A. The crystal structure showed that hydrophobic interactions as well as cation-π interactions with aromatic amino acid residues appeared to play a major role in the binding of paraherquamide A to *Ls*-AChBP (Figure 3C). However, amino acids involved in such interactions (Trp53 at Loop D, Tyr89 at Loop A, Trp143 at Loop B, and Tyr185 and Tyr192 at Loop C) are conserved through the ACR-16, UNC-38, UNC-29, UNC-63, LEV-8 and LEV-1 subunits (Figure 3A). Therefore, such interactions might underpin the L-type (UNC-38/UNC-29/UNC-63/LEV-1/LEV-8) nAChR selectivity only when the overall conformation of the orthosteric site is the dominant determinant of the affinity the

Molecular Pharmacology Fast Forward. Published on March 22, 2023 as DOI: 10.1124/molpharm.122.000601
This article has not been copyedited and formatted. The final version may differ from this version.

compound.

Paraherquamide A interacts via water with the hydroxy group of Ser186 and the main chain of Cys187 in loop C as well as the hydroxy group of Tyr164 in loop F in the crystal structure (Figure 3C, D). In accord with this finding, exchanging loop C between the ACR-16 (N-type nAChR) and UNC-38 (L-type nAChR) or UNC-63 subunits (L-type nAChR) led to a change of paraherquamide A potency on the N- and L-type nAChRs (Figure 4B, D), suggesting a contribution of the proline in loop C to determining the paraherquamide A actions. The V138E mutation in ACR-16 and E142V mutation in UNC-38 respectively enhanced and reduced the blocking potency of paraherquamide A on the N-type and L-type nAChRs (Figure 4F, H), demonstrating that the bridgehead nitrogen of paraherquamide A, when protonated, interacts electrostatically with the negatively charged glutamate in loop E of the UNC-38 subunit in the L-type nAChR, thereby strengthening the binding of the ligand. Derquantel was much less potent than paraherquamide A on the *C. elegans* L-type (UNC-38/UNC-29/UNC-63/LEV-1/LEV-8) nAChR (Figure S4) in accordance with the homology model of the *Ls*-AChBP in complex with the compound, where the lack of the carbonyl group resulted in a loss of hydrogen bonds with loop C and loop F (Figure S9).

The model of the N-type nAChR in complex with paraherquamide A (Figure 6)

Molecular Pharmacology Fast Forward. Published on March 22, 2023 as DOI: 10.1124/molpharm.122.000601
This article has not been copyedited and formatted. The final version may differ from this version.

indicated that Phe184 in loop D of the ACR-16 may prevent the compound interactions with the orthosteric site by steric contacts with Asp210. Hence, we examined the effects of F184V mutation in the ACR-16 subunit of the N-type nAChR and inverse mutations of the corresponding valines in the UNC-29 and LEV-1 subunits (V193F mutation in UNC-29 and V201F mutation in LEV-1) in the L-type nAChR on the blocking potency of paraherquamide A. We found that the F184V mutation in ACR-16 increased pIC_{50}, while the V193F mutation in UNC-29 and V201F mutation in LEV-1 decreased it (Figure 7, Table 1), supporting our hypothesis. It is therefore conceivable that loop C, loop E and loop F cooperatively determine the antagonist actions of the compound.

We investigated the actions of (-)-nicotine and levamisole on the wild type and mutant N-type and L-type nAChRs (Figure 5, Figure S7). All the mutations in loop C and E tested abolished the agonist activity of (-)-nicotine on the N-type nAChR (Figure 5A, B), while the mutation in loop F had no clear impact on the agonist activity of the compound (Figure S7A). On the other hand, none of the mutations in loop C and loop E of the UNC-38 and UNC-63 subunits as well as of the mutations in loop F of the UNC-29 and LEV-1 enabled activation by (-)-nicotine of the L-type nAChR (Figure 5B, Figure S7B). Also, all the mutations of the N-type nAChRs failed to make levamisole an agonist (Figure 5C) and the mutations of the L-type nAChR had a limited impact on the agonist

Molecular Pharmacology Fast Forward. Published on March 22, 2023 as DOI: 10.1124/molpharm.122.000601
This article has not been copyedited and formatted. The final version may differ from this version.

activity of levamisole and the antagonist potency paraherquamide A for the agonist action of levamisole (Figure 5D, E, F, G, H, Figure S7B, Table S1), suggesting differences in the modes of actions at the orthosteric site between (-)-nicotine, levamisole and paraherquamide A.

In conclusion, we have co-crystallized the *Ls*-AChBP with paraherquamide A to elucidate determinants underpinning the L-type nAChR selectivity of the anthelmintic compound. We have shown for the first time that structural features of loop C, loop E and loop F account for the L-type nAChR selectivity of paraherquamide A. Although other features, notably interactions either with non-competitive site or differential interactions with α/α vs α/α subunit interfaces, cannot be ruled out from the mechanism of selectivity, the results offer new insights into the mode of action of paraherquamide A and a platform to assist in the design of new drugs targeting cholinergic neurotransmission of parasitic nematodes.

Molecular Pharmacology Fast Forward. Published on March 22, 2023 as DOI: 10.1124/molpharm.122.000601
This article has not been copyedited and formatted. The final version may differ from this version.

Acknowledgements

The authors are indebted to Dr. Steven Buckingham, School of Biological & Chemical Sciences, Queen Mary University of London, for advice on oocyte expression. We acknowledge Prof. Thomas Boulin for the gift of the cDNAs of *C. elegans* L-type nAChR subunits and auxiliary proteins RIC-3, UNC-50 and UNC-74. The synchrotron radiation experiments were performed at the BL26B1 of SPring-8, with approvals of the Japan Synchrotron Radiation Research Institute (JASRI) (Proposal numbers: 2017A2514, 2018A2566).

Data availability

All data supporting the findings in this study are available upon request.

Authorship Contributions

Participated in research design: Koizumi, Otsubo, Furutani, Niki, Ihara, Sattelle, Matsuda.

Conducted experiments: Koizumi, Otsubo, Furutani, Niki, Takayama, Fujimura, Maekawa, Koyari, Ihara, Kai, Hayashi, Ali, Kage-Nakadai, Matsuda.

Performed data analysis: Koizumi, Otsubo, Furutani, Niki, Koyari, Ihara, Matsuda

Wrote or contributed to the writing of the manuscript: Koizumi, Otsubo, Furutani, Niki, Ihara, Kai, Hayashi, Kage-Nakadai, Ihara, Sattelle, Matsuda

Molecular Pharmacology Fast Forward. Published on March 22, 2023 as DOI: 10.1124/molpharm.122.000601
This article has not been copyedited and formatted. The final version may differ from this version.

References

Ballivet M, Alliod C, Bertrand S and Bertrand D (1996) Nicotinic acetylcholine receptors in the nematode *Caenorhabditis elegans*. *J Mol Biol* **258**(2): 261-269.

Bennett HM, Lees K, Harper KM, Jones AK, Sattelle DB, Wonnacott S and Wolstenholme AJ (2012) *Xenopus laevis* RIC-3 enhances the functional expression of the *C. elegans* homomeric nicotinic receptor, ACR-16, in *Xenopus* oocytes. *J Neurochem* **123**(6): 911-918.

Blanchard A, Guegnard F, Charvet CL, Crisford A, Courtot E, Sauve C, Harmache A, Duguet T, O'Connor V, Castagnone-Sereno P, Reaves B, Wolstenholme AJ, Beech RN, Holden-Dye L and Neveu C (2018) Deciphering the molecular determinants of cholinergic anthelmintic sensitivity in nematodes: When novel functional validation approaches highlight major differences between the model *Caenorhabditis elegans* and parasitic species. *PLoS Pathog* **14**(5): e1006996.

Blanchflower SE, Banks RM, Everett JR, Manger BR and Reading C (1991) New paraherquamide antibiotics with anthelmintic activity. *J Antibiot (Tokyo)* **44**(5): 492-497.

Boulin T, Gielen M, Richmond JE, Williams DC, Paoletti P and Bessereau JL (2008) Eight genes are required for functional reconstitution of the *Caenorhabditis*

elegans levamisole-sensitive acetylcholine receptor. *Proc Natl Acad Sci U S A* **105**(47): 18590-18595.

Buxton SK, Charvet CL, Neveu C, Cabaret J, Cortet J, Peineau N, Abongwa M, Courtot E, Robertson AP and Martin RJ (2014) Investigation of acetylcholine receptor diversity in a nematode parasite leads to characterization of tribendimidine- and derquantel-sensitive nAChRs. *PLoS Pathog* **10**(1): e1003870.

daCosta CJ, Free CR and Sine SM (2015) Stoichiometry for α-bungarotoxin block of α7 acetylcholine receptors. *Nat Commun* **6**: 8057.

Emsley P and Cowtan K (2004) Coot: model-building tools for molecular graphics. *Acta Crystallogr D Biol Crystallogr* **60**(Pt 12 Pt 1): 2126-2132.

Evans PR and Murshudov GN (2013) How good are my data and what is the resolution? *Acta Crystallogr D Biol Crystallogr* **69**(Pt 7): 1204-1214.

Ihara M, Okajima T, Yamashita A, Oda T, Asano T, Matsui M, Sattelle DB and Matsuda K (2014) Studies on an acetylcholine binding protein identify a basic residue in loop G on the β1 strand as a new structural determinant of neonicotinoid actions. *Mol Pharmacol* **86**(6): 736-746.

Jones AK, Davis P, Hodgkin J and Sattelle DB (2007) The nicotinic acetylcholine receptor gene family of the nematode *Caenorhabditis elegans*: an update on

nomenclature. *Invert Neurosci* **7**(2): 129-131.

Kabsch W (2010) Xds. *Acta Crystallogr D Biol Crystallogr* **66**(Pt 2): 125-132.

Katoh K, Misawa K, Kuma K and Miyata T (2002) MAFFT: a novel method for rapid multiple sequence alignment based on fast Fourier transform. *Nucleic Acids Res* **30**(14): 3059-3066.

Katoh K and Standley DM (2013) MAFFT multiple sequence alignment software version 7: improvements in performance and usability. *Mol Biol Evol* **30**(4): 772-780.

Lee BH, Clothier MF, Dutton FE, Nelson SJ, Johnson SS, Thompson DP, Geary TG, Whaley HD, Haber CL, Marshall VP, Kornis GI, McNally PL, Ciadella JI, Martin DG, Bowman JW, Baker CA, Coscarelli EM, Alexander-Bowman SJ, Davis JP, Zinser EW, Wiley V, Lipton MF and Mauragis MA (2002) Marcfortine and paraherquamide class of anthelmintics: discovery of PNU-141962. *Curr Top Med Chem* **2**(7): 779-793.

Matsuda K, Buckingham SD, Freeman JC, Squire MD, Baylis HA and Sattelle DB (1998) Effects of the α subunit on imidacloprid sensitivity of recombinant nicotinic acetylcholine receptors. *Br J Pharmacol* **123**(3): 518-524.

McCoy AJ (2007) Solving structures of protein complexes by molecular replacement with Phaser. *Acta Crystallogr D Biol Crystallogr* **63**(Pt 1): 32-41.

Murshudov GN, Skubák P, Lebedev AA, Pannu NS, Steiner RA, Nicholls RA, Winn MD, F. L and A. VA (2011) *REFMAC5* for the refinement of macromolecular crystal structures. *Acta Cryst* **D67**: 355-367.

Ondeyka JG, Goegelman RT, Schaeffer JM, Kelemen L and Zitano L (1990) Novel antinematodal and antiparasitic agents from *Penicillium charlesii*. I. Fermentation, isolation and biological activity. *J Antibiot (Tokyo)* **43**(11): 1375-1379.

Ostlind DA, Mickle WG, Ewanciw DV, Andriuli FJ, Campbell WC, Hernandez S, Mochales S and Munguira E (1990) Efficacy of paraherquamide against immature *Trichostrongylus colubriformis* in the gerbil (*Meriones unguiculatus*). *Res Vet Sci* **48**(2): 260-261.

Raymond V, Mongan NP and Sattelle DB (2000) Anthelmintic actions on homomer-forming nicotinic acetylcholine receptor subunits: chicken α7 and ACR-16 from the nematode *Caenorhabditis elegans*. *Neuroscience* **101**(3): 785-791.

Robertson AP, Bjorn HE and Martin RJ (1999) Resistance to levamisole resolved at the single-channel level. *FASEB J* **13**(6): 749-760.

Robertson AP, Clark CL, Burns TA, Thompson DP, Geary TG, Trailovic SM and Martin RJ (2002) Paraherquamide and 2-deoxy-paraherquamide distinguish cholinergic

receptor subtypes in Ascaris muscle. *J Pharmacol Exp Ther* **302**(3): 853-860.

Schaeffer JM, Blizzard TA, Ondeyka J, Goegelman R, Sinclair PJ and Mrozik H (1992) [^{3}H]paraherquamide binding to *Caenorhabditis elegans*. Studies on a potent new anthelmintic agent. *Biochem Pharmacol* **43**(4): 679-684.

Thompson DP, Klein RD and Geary TG (1996) Prospects for rational approaches to anthelmintic discovery. *Parasitology* **113 Suppl**: S217-238.

Trott O and Olson AJ (2010) AutoDock Vina: improving the speed and accuracy of docking with a new scoring function, efficient optimization, and multithreading. *J Comput Chem* **31**(2): 455-461.

Wallace AC, Laskowski RA and Thornton JM (1996) LIGPLOT: a program to generate schematic diagrams of protein-ligand interactions. *Protein Eng* **8**: 127-134.

Webb B and Sali A (2016) Comparative protein structure modeling using MODELLER. *Curr Protoc Bioinformatics* **54**: 5 6 1-5 6 37.

Winn MD, Ballard CC, Cowtan KD, Dodson EJ, Emsley P, Evans PR, Keegan RM, Krissinel EB, Leslie AG, McCoy A, McNicholas SJ, Murshudov GN, Pannu NS, Potterton EA, Powell HR, Read RJ, Vagin A and Wilson KS (2011) Overview of the CCP4 suite and current developments. *Acta Crystallogr D Biol Crystallogr* **67**(Pt 4): 235-242.

Molecular Pharmacology Fast Forward. Published on March 22, 2023 as DOI: 10.1124/molpharm.122.000601
This article has not been copyedited and formatted. The final version may differ from this version.

Yamazaki M, Okuyama E, Kobayashi M and Inoue H (1981) The structure of paraherquamide, a toxic metabolite from *Penicillium paraherquei*. *Tetrahedron Lett* **22**: 135-136.

Zinser EW, Wolf ML, Alexander-Bowman SJ, Thomas EM, Davis JP, Groppi VE, Lee BH, Thompson DP and Geary TG (2002) Anthelmintic paraherquamides are cholinergic antagonists in gastrointestinal nematodes and mammals. *J Vet Pharmacol Ther* **25**(4): 241-250.

Footnotes

K.M. and M.I. were supported by Grant-in-Aid for Scientific Research (KAKENHI) from the Japan Society for the Promotion of Science (Grant 21H04718 (KM); 22H02350 (MI)). D.B.S. was supported by an MRC Programme grant (Grant MR/N024842/1) on which he is Co-PI.

No author has an actual or perceived conflict of interest with the contents of this article.

Molecular Pharmacology Fast Forward. Published on March 22, 2023 as DOI: 10.1124/molpharm.122.000601
This article has not been copyedited and formatted. The final version may differ from this version.

Figure legends

Figure 1. Paraherquamide A and its effects on *C. elegans* N-type and L-type nicotinic acetylcholine receptors (nAChRs) expressed in *X. laevis* oocytes. Paraherquamide A (**A**) was bath-applied at 10 μM and 100 nM to oocytes expressing the N-type (**B**) and L-type (**C**) nAChR, respectively, for 1 min and then co-applied with 100 μM ACh (**B, C**). Paraherquamide A reduced the ACh-response of N-type and L-type nAChRs (n = 5). (**D**, **E**) Concentration-inhibitory action relationships for paraherquamide A on the N-type (**D**) and L-type (**E**) nAChRs. (**F**, **G**) Effects of paraherquamide A on the concentration-agonist action relationships for ACh on the N-type (**F**) and L-type (**G**) nAChRs. (**H**−**K**) Concentration-agonist action relationships of ACh (**H**, **I**) and concentration-inhibitory antagonist actions of paraherquamide A (**J**, **K**) on *C. elegans* 2.1 and 2.2 L-type nAChRs. Each data plot represents the mean ± standard error of mean (n = 5).

Figure 2. Actions of paraherquamide A on wild type and mutant *C. elegans.* (**A**) Wild type (N2). (**B**) Mutant (RB918 *acr-16* (*ok789*) V). (**C**) Mutant (ZZ37 *unc-63* (*x37*) I). Each data plot represents the mean ± standard error of the mean (n = 5).

Molecular Pharmacology Fast Forward. Published on March 22, 2023 as DOI: 10.1124/molpharm.122.000601
This article has not been copyedited and formatted. The final version may differ from this version.

Figure 3. Crystal structure of *Ls*-AChBP complexed with paraherquamide A.

(**A**) Amino sequences of the N-terminal domain of *C. elegans* nAChR subunits and the *Ls*-AChBP. Positions of amino acids unique to the L-type nAChR subunits are indicated by ▼ (**B**) Side View of the complex in which paraherquamide A molecules bound at five subunit interfaces. Paraherquamide A is shown with electron density maps (omit map at contour level of RMSD 3.0). (**C**) LigPlot of paraherquamide A interactions with amino acid residues or main chains in the *Ls*-AChBP. Carbons, nitrogens and oxygens are colored black, blue and red respectively, while water is colored cyan. Tyr89 (loop A), Trp53 (loop D) and Tyr192 (loop C) made hydrophobic contacts. Tyr164 (loop F), Ser186 (loop C) and the main chain nitrogen of Cys187 (loop C) formed hydrogen bonds with a carbonyl oxygen in paraherquamide A. Dashed lines indicate hydrogen bonds. (**D, E**) Close views of the interactions of the *Ls*-AChBP with paraherquamide A. (**D**) Hydrogen bonds shown by dashed lines were observed between Tyr164, Ser186, the main chain of Cys187 and one of the carbonyl groups in paraherquamide A via water. (**E**) Met114 (loop E) located in the vicinity of the bridgehead nitrogen arrowed in paraherquamide A. The principal and complementary chains are colored green and cyan, respectively, while carbons, nitrogens, oxygens, sulfur and water are colored grey, blue, red, yellow and skyblue, respectively. The bridgehead nitrogen is arrowed.

Molecular Pharmacology Fast Forward. Published on March 22, 2023 as DOI: 10.1124/molpharm.122.000601
This article has not been copyedited and formatted. The final version may differ from this version.

Figure 4. Effects of mutations in loop C and loop E on agonist actions of ACh and antagonist actions of paraherquamide A on the ACh induced response of the *C. elegans* N-type and L-type nAChRs expressed *X. laevis* oocytes. (**A** and **B**) Effects of the mutations in loop C on the actions of ACh (**A**) and paraherquamide A (**B**) on the wild type and mutant N-type nAChR. (**C** and **D**) Effects of the mutations in loop C on the actions of ACh (**C**) and paraherquamide A (**D**) on the wild type and mutant L-type nAChR. (**E** and **F**) Effects of the mutations in loop E on the actions of ACh (**E**) and paraherquamide A (**F**) on the wild type and mutant N-type nAChR. (**G** and **H**) Effects of the mutations in loop E on the actions of ACh (**G**) and paraherquamide A (**H**) on the wild type and mutant L-type nAChR. Each plotted point is mean ± standard error of the mean (n = 5). Each data plot indicates the mean ± standard error of mean (n = 5). ACh concentrations: For wild type N-type nAChRs, 10 μM; for YPSCC mutant N-type nAChR,100 μM; for V138E mutant N-type nAChR and YPCC mutant N-type nAChR, 500 μM; for wild type and mutant L-type nAChRs, 30 μM.

Molecular Pharmacology Fast Forward. Published on March 22, 2023 as DOI: 10.1124/molpharm.122.000601
This article has not been copyedited and formatted. The final version may differ from this version.

Figure 5. Effects of mutations in loop C and loop E on the actions of (-)-nicotine and levamisole on the *C. elegans* N- and L-type nAChRs expressed *X. laevis* oocytes and antagonist actions of paraherquamide A on the levamisole induced response of the L-type nAChR. (**A**) Actions of (-)-nicotine on the wild type and mutant N-type nAChRs. (**B**) Actions of (-)-nicotine on the wild type and mutant L-type nAChRs. (**C**) Actions of levamisole on the on the wild type and mutant N-type nAChRs. (**D**) Actions of levamisole on the wild type and mutant L-type AChRs. (**E**, **F**) Effects of mutations in loop C (**E**) and loop E (**F**) on the agonist action of levamisole on the L-type nAChR. (**G**, **H**) Effects of mutations in loop C (**G**) and loop E (**H**) on the antagonist action of paraherquamide A for the levamisole-induced response of the L-type nAChRs. The antagonist potency of paraherquamide A was determined for the nAChR response to 10 μM levamisole. In (**E**), (**F**), (**G**) and (**H**), each plot shows the mean ± standard error of the mean (n = 5).

Molecular Pharmacology Fast Forward. Published on March 22, 2023 as DOI: 10.1124/molpharm.122.000601
This article has not been copyedited and formatted. The final version may differ from this version.

Figure 6. Homology model of the *C. elegans* wild type N-type nAChR in complex with paraherquamide A. The main chain in the principal and complementary side of the N-type nAChRs are colored green and cyan, respectively, while carbons, nitrogens, oxygens and sulfur are colored grey, blue, red and yellow, respectively. In paraherquamide A, carbons, nitrogens and oxygens are colored grey, blue and red, respectively.

Figure 7. Effects of mutations in loop F on agonist actions of ACh and antagonist actions of paraherquamide A on the Ach-induced responses of *C. elegans* N-type and L-type nAChRs expressed *X. laevis* oocytes. Each plotted point is mean ± standard error of the mean (n = 5). (**A, B**) Effects of F184V mutation in loop F of the ACR-16 subunit on the actions of ACh (**A**) and paraherquamide A (**B**) on the N-type nAChR. (**C**, **D**) Effects of V193F and F201F mutations in loop F of the UNC-29 and LEV-1 subunits, respectively, on the actions of ACh (**C**) and paraherquamide A (**D**) on the L-type nAChR. Each plot represents the mean ± standard error of the mean (n = 5). In **B** and **D**, antagonist actions of paraherquamide A were determined for the responses to 10 μM ACh of the N-type nAChRs and 30 μM ACh of the L-type nAChRs.

Molecular Pharmacology Fast Forward. Published on March 22, 2023 as DOI: 10.1124/molpharm.122.000601
This article has not been copyedited and formatted. The final version may differ from this version.

Table 1. Agonist actions of acetylcholine and antagonist actions of paraherquamide A on acetylcholine for the *Caenorhabditis elegans* N-type and L-type nAChRs expressed in *Xenopus laevis* oocytes[a]

	Acetylcholine	Paraherquamide A[b,c]
	pEC_{50}	pIC_{50}
N-Type nAChR		
Wild type	4.67 (4.63 − 4.70)	4.84 (4.76 − 4.91)
YPSCC (loop C)	4.01 (3.95 − 4.06)*[d]	5.28 (5.20 − 5.36)*
YPCC (loop C)	3.34 (3.30 − 3.37)*	5.54 (5.43 − 5.65)*
V138E (loop E)	3.24 (3.16 − 3.33)*	5.21 (5.11 − 5.31)*
F184V (loop F)	4.72 (4.64 − 4.81)	5.45 (5.30 − 5.59)*
L-Type nAChR		
Wild type	4.39 (4.34 − 4.44)	7.58 (7.51 − 7.64)
YDCC (loop C, UNC-38)	4.37 (4.31 − 4.44)	7.37 (7.28 − 7.47)*
YDCC (loop C, UNC-63)	4.48 (4.42 − 4.53)	7.31 (7.23 − 7.38)*
E142V (loop E, UNC-38)	4.23 (4.17 − 4.30)*	7.15 (7.03 − 7.27)*
V193F (loop F, UNC-29)	4.41 (4.34 − 4.47)	6.87 (6.80 − 6.93)*
V201F (loop F, LEV-8)	4.40 (4.33 − 4.48)	7.06 (6.97 − 7.14)*
2.1	4.31 (4.24 − 4.39)	6.91 (6.79 − 7.03)*
2.2	4.82 (4.74 − 4.90)*	6.94 (6.80 − 7.08)*

[a]Data are shown as the mean (95% confidence interval (CI)) (n = 5).

[b]Paraherquamide A was >95% pure by HPLC analysis (See Supporting information).

[c]For wild type and F184V mutant N-type nAChRs, 10 μM; for YPSCC mutant N-type nAChR,100 μM; for V138E mutant N-type nAChR and YPCC mutant N-type nAChR, 500 μM; for wild type and mutant L-type nAChRs, 30 μM.

[d]Asterisk (*) indicates that difference from the wild type nAChR is significant ($P < 0.05$, one-way ANOVA, Dunnett test).

Molecular Pharmacology Fast Forward. Published on March 22, 2023 as DOI: 10.1124/molpharm.122.000601
This article has not been copyedited and formatted. The final version may differ from this version.

Table 2. X-ray diffraction data for the *Ls*-AChBP-paraherquamide A complex

PDB ID	7DJI
Beamline	SPring-8 BL26B1
Wavelength(Å)	1.0
Space group	P65
Cell dimensions a, c (Å)	74.373, 349.595
Resolution(Å)[a]	47.37 - 2.20 (2.26-2.20)
Unique reflections[a]	55263 (4552)
R_{merge}[a]	0.710 (0.713)
R_{pim}[a]	0.033 (0.436)
R_{meas}[a]	0.078 (0.841)
$CC_{1/2}$[a]	0.999 (0.0806)
I/σ[a]	21.7 (2.7)
Completeness (%)[a]	100.0 (100.0)
Redundancy[a]	10.8 (7.1)
Refinement	
Resolution(Å)[a]	47.374 – 2.200 (2.257 – 2.200)
No. of reflections[a]	55135 (3906)
Completeness (%)[a]	99.94 (99.98)
R/R_{free}(%)[a]	0.185 / 0.231 (0.268/0.295)
RMSD Bond length (Å)/angles(deg)	0.0057 / 0.224
Average B factor for all atoms	49.02
Average B factor for protein atoms	52.55
Average B factor for bound ligands	49.90

[a]Values in parenthesis represent those for most outer shell.

Molecular Pharmacology Fast Forward. Published on March 22, 2023 as DOI: 10.1124/molpharm.122.000601
This article has not been copyedited and formatted. The final version may differ from this version.

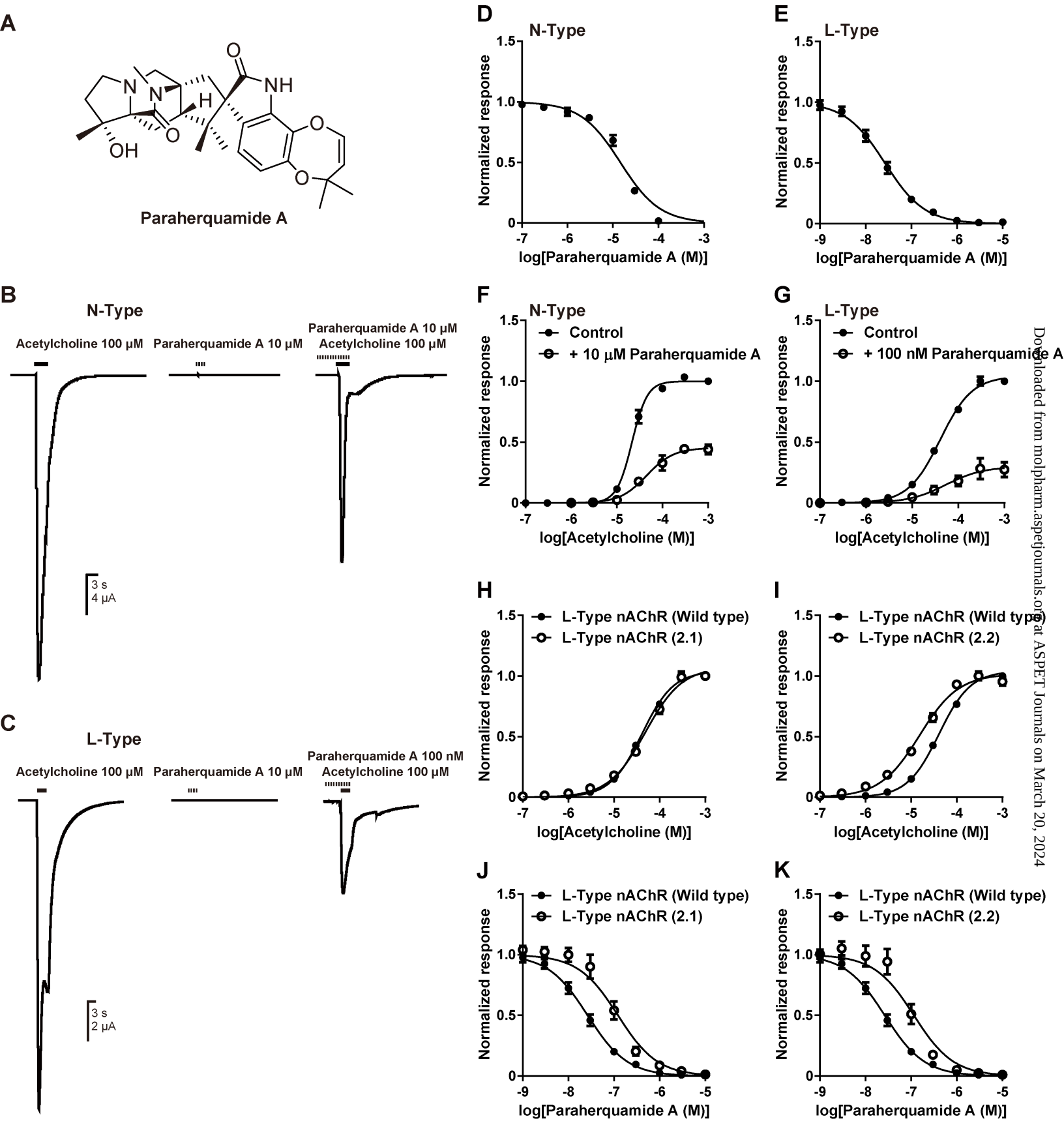

Figure 1

Molecular Pharmacology Fast Forward. Published on March 22, 2023 as DOI: 10.1124/molpharm.122.000601
This article has not been copyedited and formatted. The final version may differ from this version.

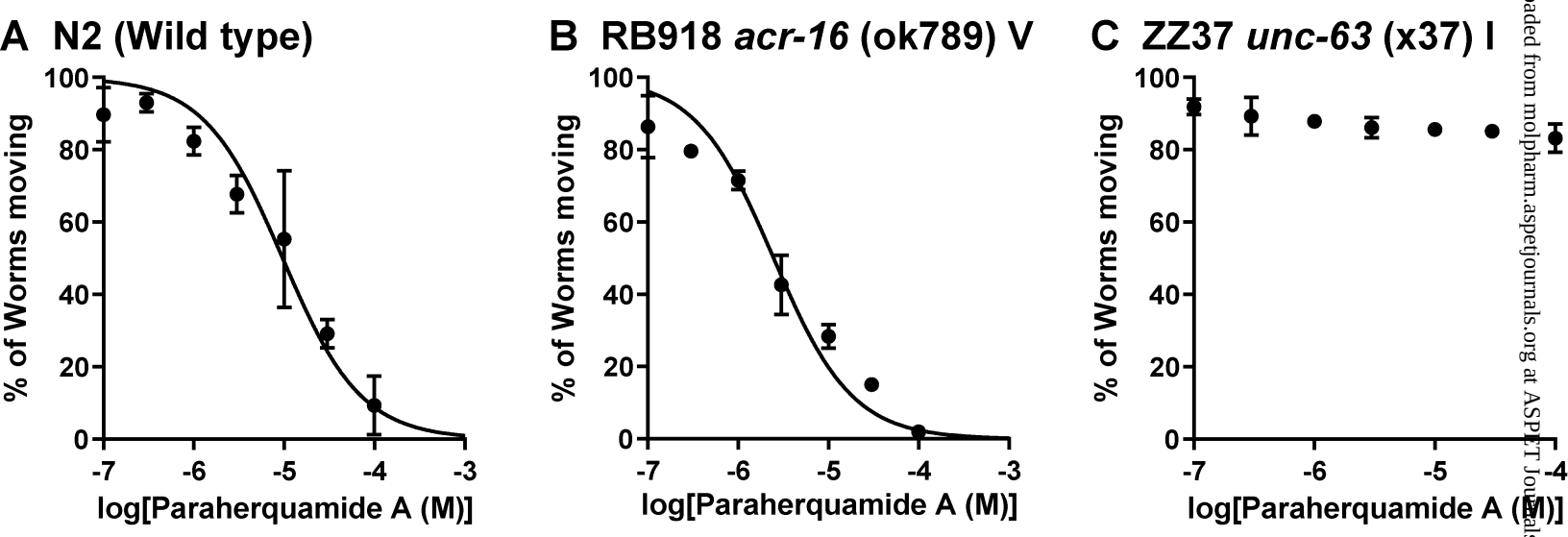

Figure 2

Molecular Pharmacology Fast Forward. Published on March 22, 2023 as DOI: 10.1124/molpharm.122.000601

A

```
AChBP     1 ----------LDRRADLLMYNIMQRSRPDVIPTQRDRPVAVSVSIKFINILEVNEITN 46
ACR-16    1 M------------------SVCTLLISCAILAAPTLGSLQERRLYEDLMRNYNNL--ERPVANHSE---PVTVHLKVALQQIIDVDEKNQ 67
UNC-38    1 M----RS-----------FWLFLLLLLFCISFIKLTEGNEDAKRLYDDLMVNYNRH--RRPSTSPNK---PLTIKLKLRLSQIIDVHEIDQ 71
UNC-63    1 MGPNDHG-----------FAYILIFLLLSPP----THANRDANRLFEDLIADYNKL--VRPVSENGE---TLVVTFKLKLSQLLDVHEKNQ 71
LEV-8     1 MWIPQRISH----------IFLLVIFILHIVTINANKHVSQLLENLLTDYNKA--VRPVHNASD---ALKVKFGANLCRLIDVDEVNQ 73
UNC-29    1 MRTNRL-------SWILVLSVVIFLVII----NTINASDDEERLMVDVFRGYNSL--IQPVRNSSEL--PLIVKMALQLVLLINVDEKDQ 75
LEV-1     1 MMLGGGGGCGAGGTW---LGFLVFLAVSLRNHSTCEDIDAEDRLMVDLFRGYNSL--VQPVRNRSEL--PMIVKIGMQLVLLINVDEKEQ 83

                  Loop D                              Loop A                    Loop E
                  ▬▬▬                                 ▬▬▬                       ▬▬▼

AChBP    47 EVDVVFWQQTTWSDRTLAWNSSH--SPDQVSVPISSLWVPDLAAYN-AISKPEVLTPQLARVVSDGEVLYMPSIRQRFSC--DVSGVDTE 131
ACR-16   68 VVYVNAWLDYTWNDYNLVWDKAEYGNITDVRFPAGKIWKPDVLLYNSVDTNFDSTYQTNMIVYSTGLVHWVPPGIFKISCKIDIQWFPFD 157
UNC-38   72 IMTCSVWLKQTWIDRKLSWDPVNYGGVNVLYVPYEMIWVPDIVLYNNADSNYNITISTKATLHYTGEVTWEPPAIFKSMCQIDVRWFPFD 161
UNC-63   72 IMTTNVWLQHSWMDYKLRWDPVEYGGVEVLYVPSDTIWLPDVVLYNNADGNYQVTIMTKAKLTYNGTVEWAPPAIYKSMCQIDVEFFPFD 161
LEV-8    74 VLTTSLWLEMQWYDKKLTWNPTDWGGVEYIHIPSDQIWIPDIVLYNNADGEPHITITSLAKIDHHGRVVWQPPSIYKSFCPINIKYFPYD 163
UNC-29   76 VMHTNVWLTLQWHDFQMKWNPVNYGEIKQIRVSPDKVWLPDIVLFNNADGNYEVSFMCNVVINHKGDMLWVPPAIYKSSCIIDVEFFPFD 165
LEV-1    84 VMHTNVWLTMKWDDFQLKWDPRDYANITQIRVAPEKVWLPDIVLFNNADGNYEVSFMCNVLILSTGTVLWVPPAIYKSSCIIDVEFFPFD 173

                  Loop B                                                Loop F                  Loop C
                  ▬▬▬                                                   ▬▬▼                     ▬▬▼

AChBP   132 SGATCRIKIGSWTHHSREISVDPTTEN-------------------------SDDSEYFSQYSRFEILDVTQKKNSVTYS-CCPEA-YE 193
ACR-16  158 E-QKCFFKFGSWTYDGYKLDLQPATGG-------------------------FDISEYISNGEWALPLTTVERNEKF-YD-CCPEP-YP 217
UNC-38  162 E-QQCHLKFGSWTFSENLLSVELNEPSLRYEEEIDEKGII----DNVTVAEDGIDLSDYYPSVEWDIMSRVAKRRAKN-YPSCCPQSAYI 245
UNC-63  162 R-QQCEMKFGSWTYGGLEVDLQHRDKHLEKEIEEDVEGVDGPTKEIVWVVDRGIDLSDYYPSVEWDILNVPGKRHSKR-YP-CCESP-FI 247
LEV-8   164 W-QTCEMKFGGWSNDGETLDLYQIPVDVDDIPQVKRQDDGVE----FLYLEKGLGLSFYHESAEWDLLSATSSRYAQI-YPGCCGQQYYI 247
UNC-29  166 E-QVCTLVFGSWTYNENEIKLEFVQAEL-------------------------VDVSEYSASSIWDVIDVPASLVNKRS---------RI 220
LEV-1   174 D-QLCSLTFGSWTYNRDEIKLDFLTSDR-------------------------VDFSEYSTSSIWDMMDGPAVLTSDRS---------RI 228
```

B

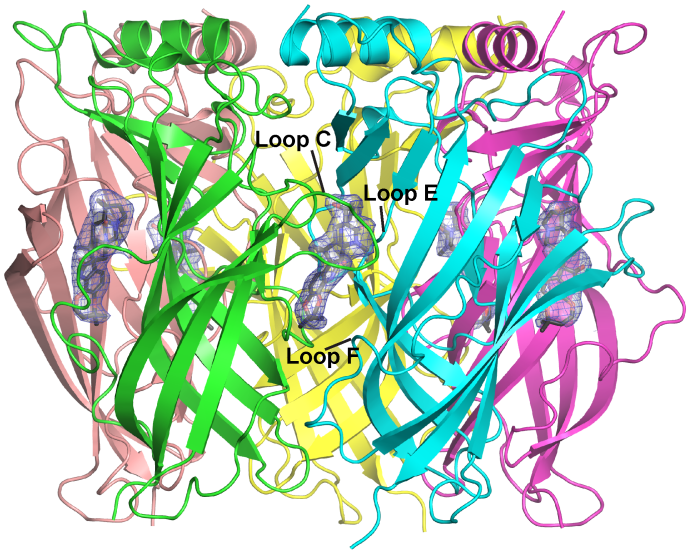

C

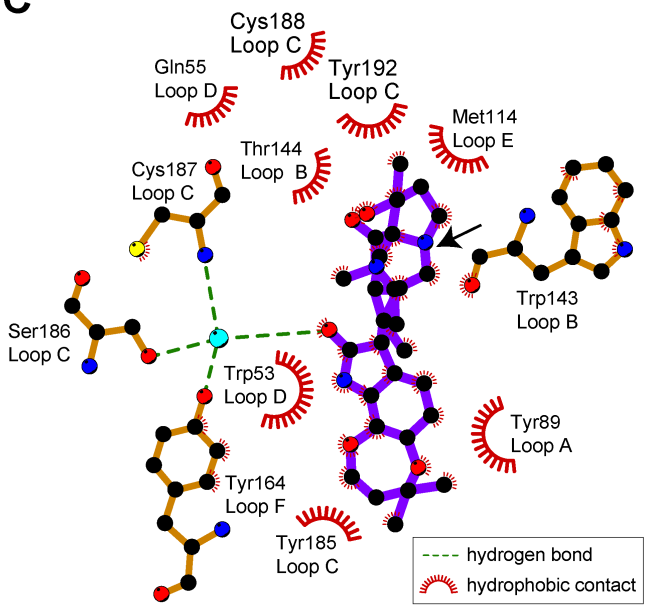

D

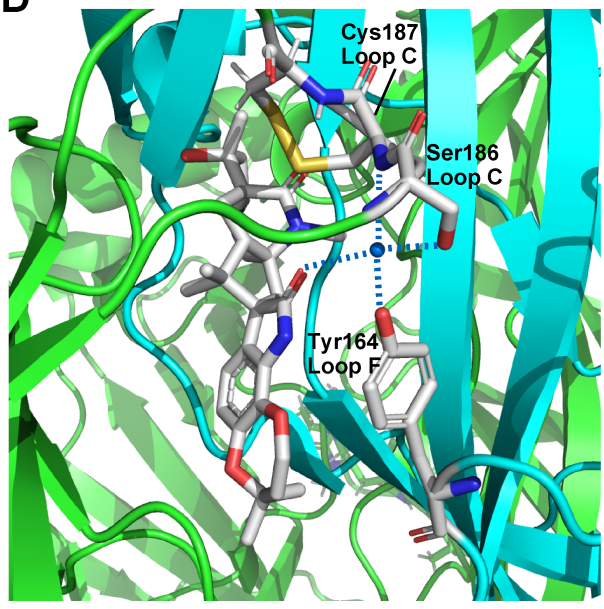

E

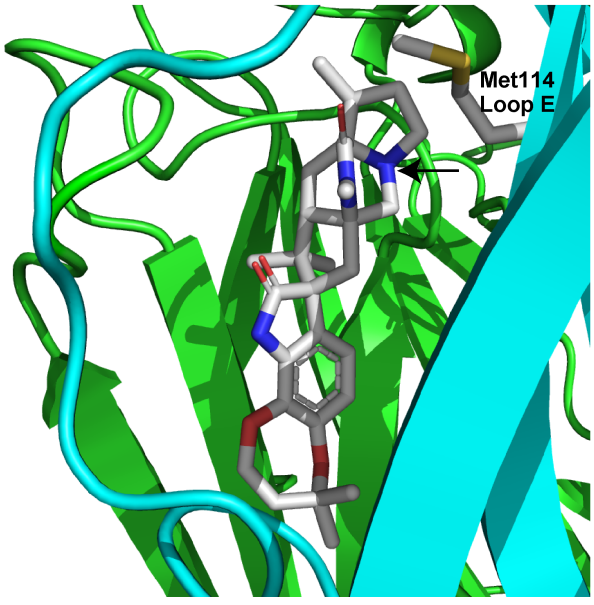

Figure 3

Molecular Pharmacology Fast Forward. Published on March 22, 2023 as DOI: 10.1124/molpharm.122.000601
This article has not been copyedited and formatted. The final version may differ from this version.

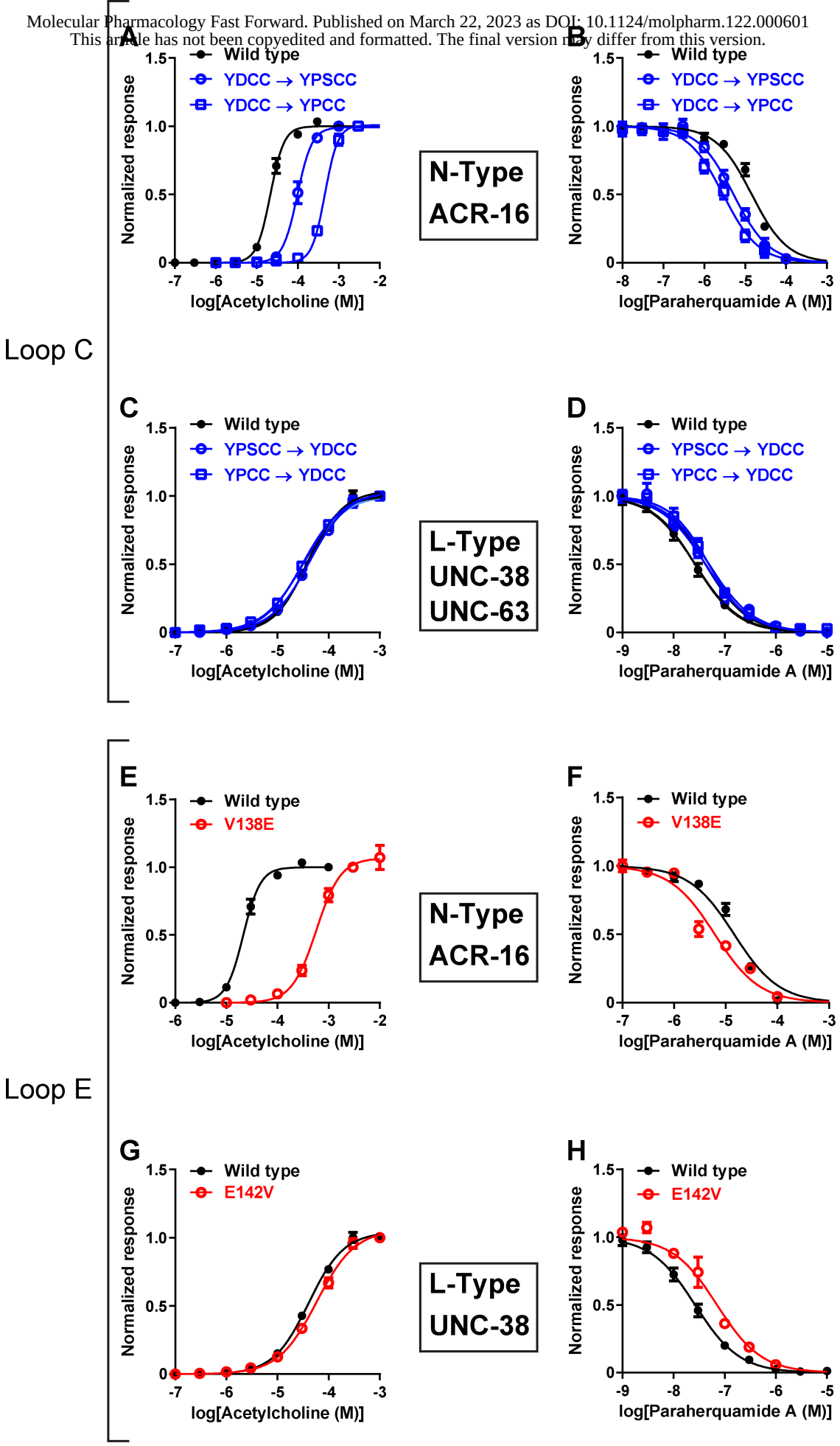

Figure 4

Molecular Pharmacology Fast Forward. Published on March 22, 2023 as DOI: 10.1124/molpharm.122.000601
This article has not been copyedited and formatted. The final version may differ from this version.

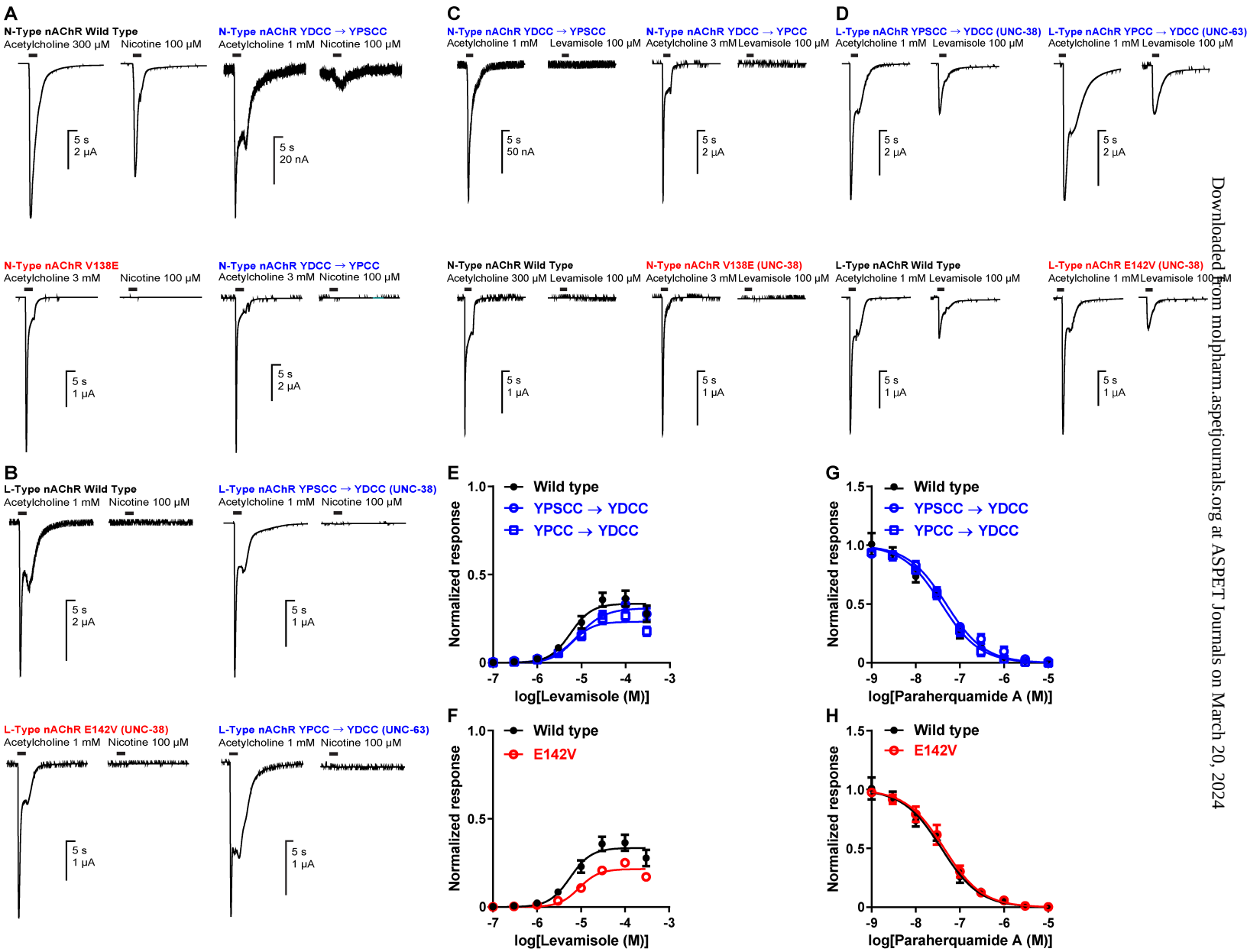

Figure 5

Molecular Pharmacology Fast Forward. Published on March 22, 2023 as DOI: 10.1124/molpharm.122.000601
This article has not been copyedited and formatted. The final version may differ from this version.

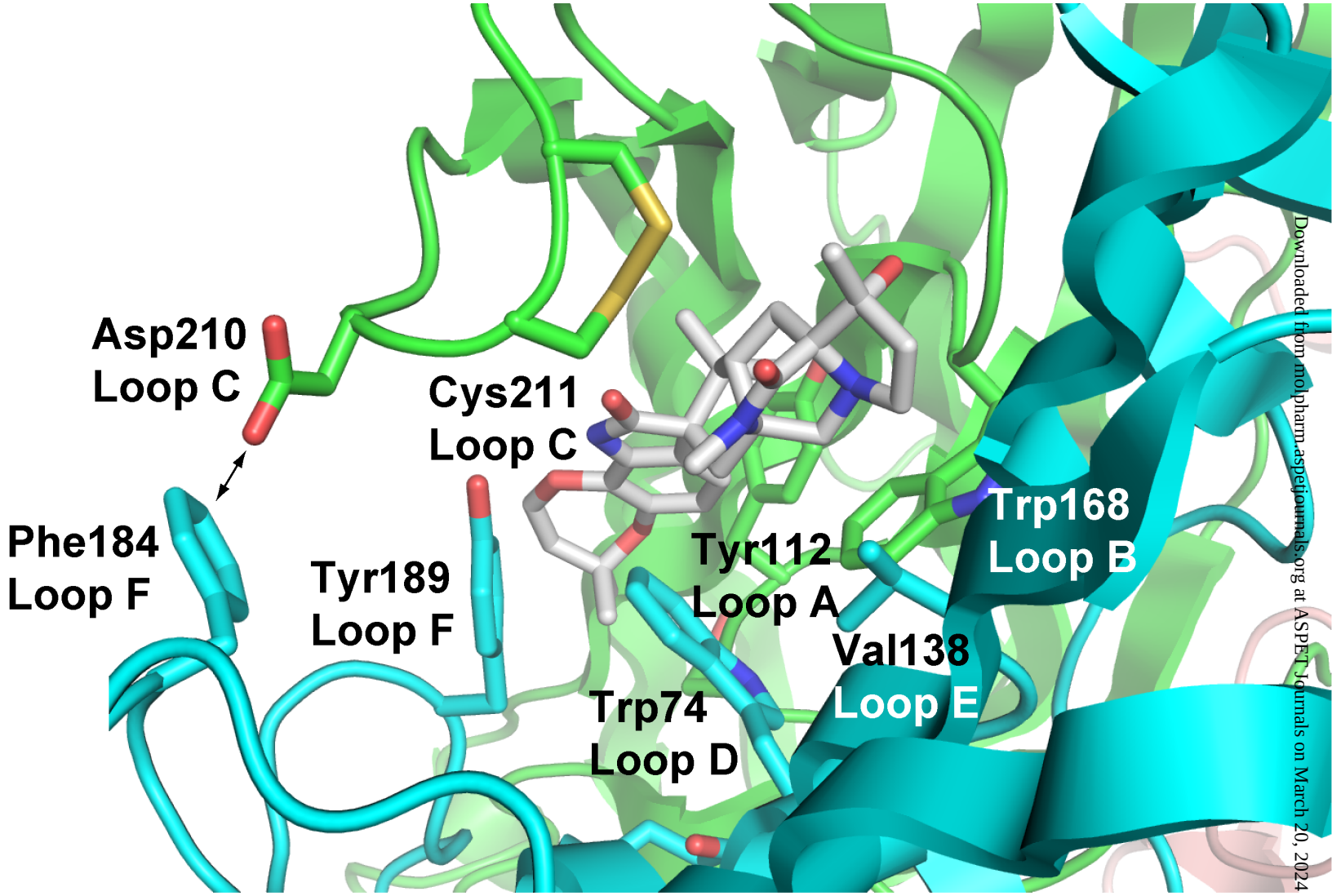

Figure 6

Molecular Pharmacology Fast Forward. Published on March 22, 2023 as DOI: 10.1124/molpharm.122.000601
This article has not been copyedited and formatted. The final version may differ from this version.

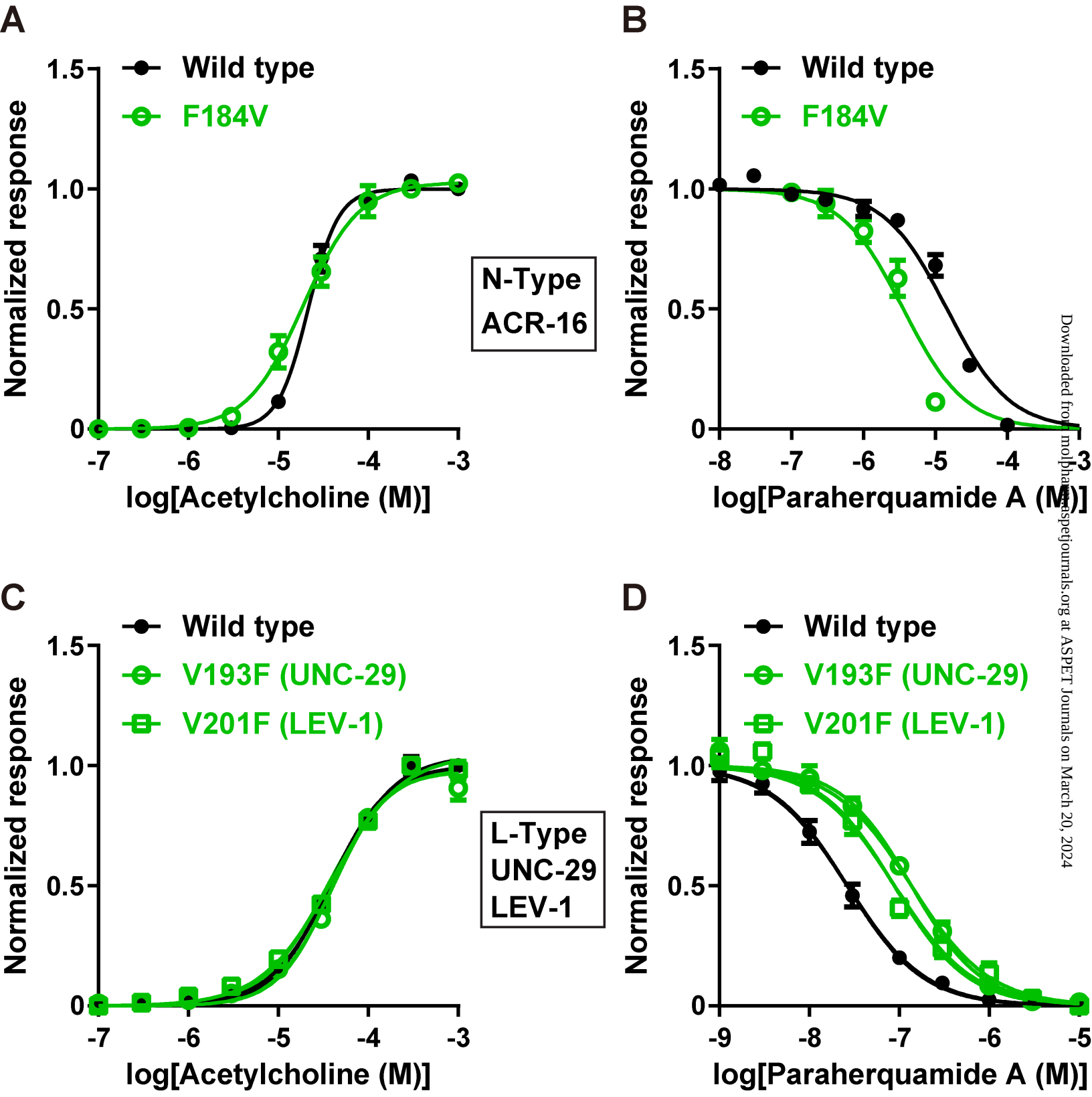

Figure 7